Differential cross sections for $H+D_2 \rightarrow HD\ (v'=2, J'=0,3,5)+D$ at 1.55 eV

Félix Fernández-Alonso, Brian D. Bean, and Richard N. Zare
Department of Chemistry, Stanford University, Stanford, California 94305

(Received 20 April 1999; accepted 17 May 1999)

The photoloc technique with core extraction of the nascent product laboratory speed distribution in a Wiley–McLaren time-of-flight spectrometer has been used to measure differential cross sections for the reaction $H+D_2 \rightarrow HD\ (v'=2, J'=0,3,5)+D$ at collision energies ~1.55 eV. We find that the peak of each angular distribution shifts from complete backward scattering toward side scattering as the rotational excitation of the product increases. We found the same trend in our previous study of $H+D_2 \rightarrow HD\ (v'=1, J'=1,5,8)+D$ at ~1.70 eV. We conclude that the same type of correlation exists between impact parameter and rotational quantum number in both product vibrational manifolds. Further analysis of the HD $(v'=2, J')$ differential cross section data reveals, however, a clear tendency of this vibrational manifold to scatter sideways at lower J' than HD$(v'=1, J')$. Within the framework of a line-of-centers model with nearly elastic specular scattering, this result implies that smaller impact parameters lead to more vibrationally excited products. © *1999 American Institute of Physics.* [S0021-9606(99)01130-7]

I. INTRODUCTION

The amount of literature devoted to the qualitative and quantitative aspects of the reaction dynamics for the hydrogen–atom hydrogen–molecule exchange reaction is vast. The reader is referred to several reviews[1–6] for further information and details regarding this subject. Despite its long history, this topic still remains of great interest for the chemical reaction dynamics community as a benchmark system for comparing theory and experiment. In a previous publication[7] we reported the measurement of rovibrationally state-resolved center-of-mass angular distributions for the reaction

$$H+D_2 \rightarrow HD\ (v'=1, J'=1,5,8)+D,$$

at 1.70 ± 0.05 eV. These differential cross sections were determined using the photoloc technique with core extraction of the nascent laboratory velocity distribution in a Wiley–McLaren time-of-flight spectrometer.[8] In this study we found that the angular distribution shifts from backward toward side scattering with increasing rotational quantum number J' of the HD $(v'=1)$ product. Based on the experimental data we proposed a line-of-centers with nearly elastic specular scattering (LOCNESS) model that links the final rotational quantum number J' of the diatomic product with initial impact parameter b. The LOCNESS model assumes the simplest deflection function for the reaction product as well as incorporates a criterion for reaction solely based on the energy available along the line of centers for a given impact parameter and collision energy. This treatment assumed that the reaction is of direct character.

As a continuation of the aforementioned work on HD$(v'=1, J')$, we have conducted additional differential cross section measurements in the HD $(v'=2, J')$ vibrational manifold at a similar but somewhat lower collision energy of 1.55 ± 0.05 eV. A preliminary measurement of the HD $(v'=2, J'=3)$ product differential cross section at this collision energy was reported in Ref. 8, but in that work we put more emphasis on the details of the experimental setup and instrument characterization procedures. Our current ability to conduct these measurements is mainly because of the practical advantages associated with the photoloc technique.[7–11]

For almost three decades several groups have attempted the measurement of state-resolved angular distributions for the hydrogen exchange reaction. Until very recently the success at achieving this goal has been rather limited. The first measurement of the total product differential cross section from the the isotopically substituted $D+H_2$ reaction at a mean collision energy of 0.48 eV was performed by Geddes, Krause, and Fite[12] in 1972. The experimental setup consisted of a crossed molecular beam chamber equipped with a high-temperature effusive furnace for hot-atom generation and an electron impact ionizer/quadrupole mass spectrometer for HD product detection. The angular distribution was found to be preferentially backward scattered, a finding consistent with available theoretical predictions at that time. Work along these lines was followed by Kwei and Lo[13] who studied the reaction of H and D atoms with T_2 molecules at 0.7 eV using an effusive hot-atom source and a MoO_3 detector for tritium detection. The HT/DT angular distributions were also found to be backward scattered. Götting, Mayne, and Toennies carried out further experiments for the $D+H_2$ reaction at collision energies of 1.0 eV[14] and 1.5 eV.[15] Hot-atom generation at these high center-of-mass collision energies was achieved by the use of an arc discharge capable of creating D-atom velocity distributions with mean energies as high as 3.0 eV. In these studies the product angular distributions were observed to shift to smaller angles with increased collision energy, in agreement with quasiclassical trajectory calculations on the Liu, Siegbahn, Truhlar, Horowitz[16,17] (LSTH) potential energy surface. By the end of the 1980's, the marriage of the crossed-beam technique with laser photolysis for hot-atom generation, and laser spectroscopy for

quantum-state-specific product detection made it possible to refine the experimental conditions to an unprecedented level of detail. The work of Buntin, Giese, and Gentry[18] using D_2S photolysis at 248 nm for D-atom generation, and Continetti, Balko, and Lee[19] employing DI photolysis at 248 nm provided the first angular distributions with some internal energy resolution of the diatomic product.

From these initial attempts, the difficulties associated with state-resolved measurements using conventional crossed-beam techniques became apparent. As a result, laser spectroscopy became the method of choice for product detection. Most recently, Schnieder and co-workers[20–23] have combined the crossed-beam technique with laser photolysis of HI and the ultrasensitive detection scheme of D-atom Rydberg tagging time-of-flight spectroscopy to perform the first fully state-resolved study of this reaction at 1.28 and 0.55 eV. The availability of this experimental data has fostered recent calculations of state-resolved angular distributions[20–27] and product rotational polarization[28] using quantum mechanical and quasiclassical methods.

In contrast with the difficulties associated with the experimental efforts listed above, the photoloc technique[8,11,29] allows conducting the experiments in a single molecular beam expansion thereby greatly reducing the complexity of the experimental setup. Reaction is initiated by photolysis of a suitable molecular precursor and angular measurements are performed by inversion of the product laboratory speed distribution into a center-of-mass differential cross section. The major prerequisites for the successful application of this technique are a knowledge of the spatial anisotropy of the photodissociation as well as velocity-sensitive, quantum-state-specific detection of the reaction product. The inversion of the laboratory speed distributions into differential cross sections is then possible by straightforward application of energy and momentum conservation along with the law of cosines which maps a single product laboratory speed onto a unique center-of-mass scattering angle. Implementation of this or similar techniques has already proven very useful for the study of several reaction systems in our and other laboratories in the past few years. These include, for example: $Cl+CH_4$,[30,31] $Cl+C_2H_6$,[32–34] $H+O_2$,[35] $O+H_2$,[36] and $H+CO_2$.[37] Some of these experiments have been successful at measuring not only state-to-state differential cross sections but also product rotational polarization,[29,38,39] and the effect of reagent vibrational excitation[40] and alignment[41] on product angular distributions. These measurements have opened a new and unexplored area in the field of experimental reaction dynamics devoted to the investigation of vector correlations in chemical reactions.

In regard to the hydrogen exchange reaction, the photoloc technique has made it possible to attain sufficient product number densities under single-collision conditions to make total[10] and rovibrational-state-resolved[7,8,42] differential cross section measurements feasible. Furthermore, the use of a quantum-state-specific spectroscopic technique such as $(2+1)$ REMPI for the detection of the HD (v', J') product permits the isolation of a particular quantum state of the product, with almost no possibility of coincidental overlaps with other product states. This ability to isolate particular HD (v', J') states is particularly useful in two situations: (1) when we want to measure the differential cross section into states that constitute a small fraction of the overall product flux, i.e., highly excited products such as HD $(v'=2, J')$; and (2) when the collision energies are sufficiently high for many HD product channels to be open, thus increasing the number of nearly isoenergetic D-atom translational states. It is for this reason that the work of Schnieder *et al.* has not been capable of providing in their high collision energy experiments at 2.2 eV[43] and 2.67 eV[44] the same amount of information as that obtained in their beautiful experiments at 1.28 and 0.55 eV. More recently, the same group has repeated the differential cross section measurements at 2.2 eV with improved internal energy resolution.[45] Despite some overlaps between different HD (v', J') product states the agreement with quantum-mechanical calculations on the Boothroyd, Keogh, Martin, Peterson[46] (BKMP2) surface is very good.

This article has been organized as follows. We first describe briefly the experimental apparatus, which remains the same in its essentials from the setup used in previous studies.[7,8] We focus on a more detailed account of the experimental protocol that enables us to measure reliable laboratory velocity distributions for product states with integral reaction cross sections calculated to be as low as 0.001 $Å^2$ (Ref. 47). In Sec. III we present the HD time-of-flight profiles as well as the angular distributions directly derived from them after incorporating the effects of instrumental resolution. In Sec. IV we compare the present results with our previous measurements in the HD $(v'=1, J')$ vibrational manifold. We also show how the HD $(v'=2, J')$ data agree closely with the predictions and expectations of the LOCNESS model, giving us further insight into the details of the dynamics of this reaction.

II. EXPERIMENT

A. Summary of the experimental procedures

A complete account of the experimental setup, instrument calibration procedures, and implementation of the photoloc technique has been given in previous publications.[7,8] In brief, a 1:4 mixture of HBr and D_2 is expanded into a vacuum chamber with the aid of a solenoid pulsed valve. Its opening is synchronized with the firing of the lasers and driven by a high-voltage solenoid driver to achieve short pulse operation.

As with previous HD $(v'=1, J')$ measurements, the same laser pulse has been utilized to photolyze the HBr precursor and to detect the nascent HD $(v'=2, J')$ product. Hence we only collect those products that are allowed to buildup during the duration of the laser pulse, whose temporal width lies between 5 and 6 ns. A practical advantage of using a single laser beam in these experiments is that there is no need to perform a signal correction to account for product flyout.

The photolysis of HBr generating two monoenergetic populations of H atoms has been previously studied at these wavelengths.[8] From this work we found that around 86% of these hydrogen atoms corresponded to the fast channel with

a spatial anisotropy of $\beta=-1$ (perpendicular transition). These findings are in excellent agreement with the most recent study of HBr photolysis by Regan *et al.*[48] who have performed a detailed study of the photodissociation dynamics of this molecule over a wide range of photolysis energies.

Product detection was accomplished via the *Q*-branch members of the HD $E,F\,^1\Sigma_g^+ - X\,^1\Sigma_g^+(0,2)$ band.[49,50] The sensitivity of this particular spectroscopic band is of a similar magnitude as the (0,1) band previously employed for the detection of HD $(v'=1, J')$ product.

Linearly polarized laser radiation around 217 nm was generated by frequency tripling the output of a pulsed dye laser pumped by the doubled output of an injection-seeded Nd:YAG laser operating at 10 Hz. Typical output laser powers ranged between 1.0 and 1.5 mJ/pulse. The beam was recollimated and focused by a 500 mm plano convex lens prior to entering the vacuum chamber. Special care was exercised to have a well-defined laser polarization entering the vacuum chamber. The purity of the polarization is crucial for a proper modeling of the core-extracted time-of-flight signals. The state of polarization of the laser light was checked before and after the reaction region to ensure that it was preserved after passing through the fused-silica chamber windows. These windows were periodically taken out of the beam line and checked for burns or spot marks produced by repeated exposure to UV radiation. The laser power was fine-controlled by a set of two UV polarizers. Careful control of the laser power proved to be crucial in these experiments because excessive laser fluences tended to produce severe distortions in the time-of-flight profiles (as explained in more detail in Sec. II B). Probing the reaction products 25–35 nozzle diameters below the nozzle orifice ensured single-collision conditions.

After photolysis and subsequent ionization, product ions travel inside a Wiley–McLaren time-of-flight spectrometer. A 3-mm-radius conical mask placed along the time-of-flight axis cores the ion packet prior to its detection by a Chevron-type microchannel plate detector. The data presented here have been taken by recording ion signals in single ion counting mode. Single ion counts in a mass window corresponding to HD (v',J') product are recorded as a function of flight time on a digital oscilloscope and sent to a personal computer for permanent storage and further analysis.

B. Improvement of experimental protocol

A smaller reaction cross section leading to HD $(v'=2, J')$ levels make the measurements presented here more challenging than those previously reported.[7] Consequently, additional care had to be exercised to remove ion backgrounds at other masses produced by the high intensity of the focused laser beam. These backgrounds arise from the breakage and further ionization of the reagents HBr and D_2, whose number densities are several orders of magnitude larger than those from the desired reaction products. Large backgrounds from D^+ and D_2^+ were very dependent on the laser power and the temporal delay between the firing of the pulsed nozzle and the laser pulse, i.e., the local beam number density. Too large ion signals at these masses, especially from the D^+ ion at $m/e=2$, tended to leak into the mass window corresponding to HD product contributing to baseline degradation and instability. Moreover, high mass ions such as HBr^+ and Br^+ arising from multiphoton dissociation and ionization of the HBr reagent were particularly detrimental to the quality and line shape of the HD^+ ion signal. Owing to the large masses of these ions, they have very long residence times in the extraction region of the time-of-flight spectrometer compared to those of the lighter reaction products. The presence of large quantities of these quasistatic ions in the extraction region caused severe distortions in the time-of-flight profiles, thus impairing the extraction of reliable velocity information. Because of the characteristics of our time-of-flight spectrometer,[8] ion peaks for a given mass should appear symmetric about the arrival time of an ion with no speed along the time-of-flight axis. This symmetry requirement served as a very useful diagnostic tool. The data presented in the next section have been measured under conditions in which all these experimental artifacts have been reduced to an acceptable level. No attempt has been made to symmetrize the time-of-flight about the zero time-of-flight delay *a posteriori* or to artificially remove spurious ion backgrounds.

TABLE I. Summary of reaction parameters pertinent to this work.

	HD $(v'=2, J')$ product		
	$J'=0$	$J'=3$	$J'=5$
Collision energy (eV)	1.56	1.55	1.53
Center-of-mass speed (m/s)	3856	3844	3826
D_2 vibrational energy (eV)	0.191	0.191	0.191
D_2 rotational energy (eV)	0.005	0.005	0.005
HD vibrational energy (eV)	1.109	1.109	1.109
HD rotational energy (eV)	0	0.060	0.148
HD center-of-mass speed (m/s)	3919	3684	3309
HD laboratory speed (m/s)			
fast	7775	7528	7136
slow	62	160	517

Once we were capable of finding reactive signal from the reaction, the laser power and reagent number densities were reduced to levels under which background ion peaks were insignificant and did not affect the product velocity distribution. This condition generally required us to operate under single-ion counting conditions, and to acquire data for time intervals of at least 20–30 min. As it was found in previous measurements of angular distributions, the optimal place to probe for nascent reaction products is located within the first 50–100 μs of the 600-μs-gas pulse. Under these operating conditions the rotational distribution of the D_2 reagent, and the collision energy spread were found to be the same as in previous experiments.

III. RESULTS

A. Reaction conditions

Table I summarizes the reaction parameters pertinent to this study. Owing to the proximity of the rotational lines used for product detection, the change in collision energy for each measurement is less than 30 meV. This value is still

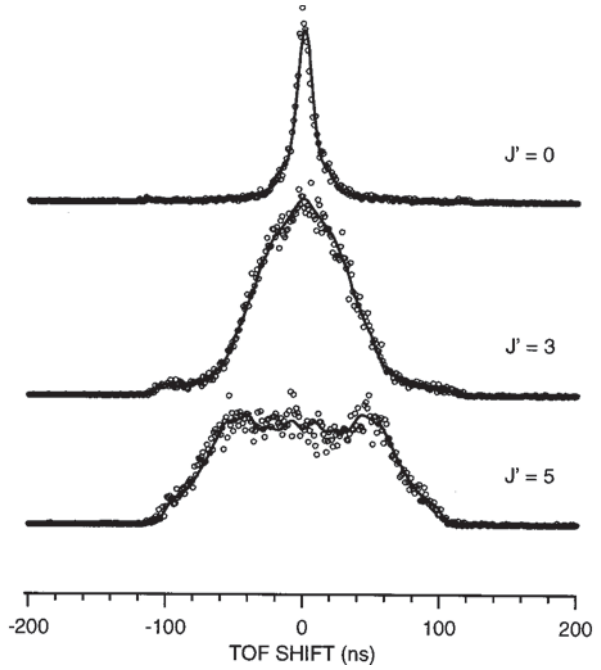

FIG. 1. Time-of-flight profiles for $H+D_2 \rightarrow HD$ ($v'=2, J'=0,3,5$) + D at collision energies ~1.55 eV. HD detection was accomplished by (2+1) REMPI through the *Q*-branch members of the (0,2) band of the HD $E,F\ ^1\Sigma_g^+ - X\ ^1\Sigma_g^+$ transition. The solid lines are least-squares fits to the experimental profiles using the basis function generation and linear least-squares methods described in the text.

within the measured collision energy spread of 50 meV. Therefore, the three states measured in this study can be considered to be at the same collision energy. The reagent and product internal energies have been calculated from the spectroscopic values of Huber and Herzberg.[51] The D_2 rotational energy shown in the fourth row of Table I is the average energy of the the rotational distribution of $J=0$, 1, and 2 levels measured by (2+1) REMPI. The HD center-of-mass speeds shown in the last two rows have been calculated from a straightforward application of energy and momentum conservation.[8] The last row shows the laboratory speed range for each product, which corresponds to complete forward and backward scattering of the reaction product in the center-of-mass frame.

Although a slower photolysis channel could contribute to reaction product, our measurements of the HBr photolysis branching ratio at these wavelengths[8] show that only 14% of this slower channel is produced under the current experimental conditions. Moreover, our probing scheme is sensitive to the state-to-state reaction rate and not to the reaction cross section. The contribution of the slow channel to the reactive signal is at most 8–10%, if we take into account the lower collision energy as well as the smaller reaction cross section.[47,52] We are thus confident that, within the uncertainties in the measurements, the velocity distributions and consequently the center-of-mass differential cross sections arise from the fast photolysis channel.

B. Core-extracted time-of-flight profiles

Figure 1 shows representative core-extracted time-of-flight profiles for HD ($v'=2, J'=0,3,5$) taken with the laser polarization perpendicular to the time-of-flight axis. Despite the expected lower cross sections for reaction compared to the HD ($v'=1, J$) product, we have been able to obtain background-free reactive product signals of comparable, if not better, quality to the HD ($v'=1, J'$) data previously presented. A more complete account of all the factors affecting the quality of the time-of-flight profiles and how we have circumvented these problems has already been given in Sec. II B.

The extraction voltage conditions used in these experiments are such that reactive signal should be found 120 ns on either side from the center of the time-of-flight profile for the three rotational states shown in Fig. 1. These expectations are clearly fulfilled by the time-of-flight profiles shown in this figure. Note the lack of any spurious background outside of the physical bounds determined from the reaction kinematics and energetics for each of these products. Also note the large degree of symmetry of the recorded data about their center. In general, distortions in the velocity distributions caused by space-charge effects initially cause a decrease of the signal arising from the late-arriving ions (i.e., signal with a positive time-of-flight shift). As the background ion production is increased, we observe an overall decrease of the ion signal but more so for those ions that spend more time in the extraction region. After a certain laser power threshold half of the profile, corresponding to the late-arriving ions, completely disappears and only a single compressed ion peak arriving at earlier times is discernible. The shift in the arrival time is small compared to the total flight time but of a sufficient magnitude to be clearly observable. We believe this peak arises from those ions that managed to escape the highly congested extraction region, receiving an overall extra push toward the detector by the large number of positive ions left behind, which naturally translates into an earlier arrival time.

The extraction voltages used to collect the signals from Fig. 1 are also the lowest compatible with measurable signal levels. They correspond to electric fields strengths of 20 V/cm (50 V drop across the 0.9–in.–long extraction region). The use of low extraction voltages has two beneficial consequences. First, it increases the velocity resolution of the instrument to a degree for which it is possible to use a relatively large number of velocity basis functions for the linear least-squares fitting of the signal. As explained in more detail in the next section, our current velocity resolution allows for the use of 12–14 velocity basis functions spanning the complete scattering angular range. The concomitant angular resolution of 5–13 degrees is comparable to the one obtainable from far more demanding experiments using the technique of crossed molecular beams. Second, low extraction voltages allow the ion cloud to expand as much as possible as it travels down the time-of-flight apparatus, making the measured profile less susceptible to shape changes caused by improper centering of the ion packet onto the core extractor. Obviously, the greatest limitation is the steep drop in the number of ions that make it through the core extractor. As the extraction voltage is lowered, the observed signal decreases approximately as the cube of the applied extraction voltage. Fortunately, the use of the very sensitive (2+1)

REMPI scheme for HD (v', J') detection in conjunction with relatively long collection times (20 000 laser shots per profile) enables us to use the Wiley–McLaren time-of-flight spectrometer at a resolution very close to the maximum one currently attainable with our experimental setup, i.e., other blurring factors such as laser pulse duration become predominant.

Because the laboratory velocity range for all three states is quite similar (cf. Table I), any differences in the shape of the profiles shown in Fig. 1 are directly attributable to differences in the center-of-mass angular distributions. It is quite fulfilling to be able to discern so clearly these differences directly from the core-extracted time-of-flight profiles without recourse to further analysis of the experimental signals. For example, the laboratory speed distribution for HD ($v'=2$, $J'=0$) is extremely narrow and centered around zero. Thus, the center-of-mass angular distribution must be preferentially backward scattered. As we move to $J'=3$ and $J'=5$ the velocity distributions become wider and flatter, which indicates that scattering becomes more sideways. Direct inversion of the time-of-flight profiles to obtain quantitative information about the center-of-mass angular distributions requires a good knowledge of the instrument function. The details of these procedures have been thoroughly described previously[8] and will be summarized in the next section.

C. Center-of-mass angular distributions

The solid lines accompanying the core-extracted time-of-flight profiles in Fig. 1 are the result of a singular-value decomposition fit[53] to the signal using twelve evenly spaced velocity basis functions. The velocity basis functions have been obtained via a Monte Carlo simulation of the instrument for a particular photolysis polarization and for ions with a fixed laboratory speed and angular anisotropy with respect to the photolysis polarization. Instrumental blurring, parameterized via the inclusion of longitudinal and lateral blurring functions, has been determined from studies of simpler processes that include O_2 photolysis,[54] HBr photolysis, and H_2 (v', J') velocity distributions arising from the H+HB*r* reaction.[8] It was very encouraging to find that our instrumental parameters could be used without further modification to fit the signals presented here.

The core-extracted time-of-flight profile for HD ($v'=2$, $J'=0$) is extremely narrow. As such, it can be regarded as a good testing ground for the accuracy of the single-speed velocity basis functions generated via the Monte Carlo simulation of the instrument. It was quite reassuring to find that our description of the instrument function could faithfully account for the width and shape of this distribution without any adjustments. For example, overestimation of the instrument function by our calibration procedures would have made it extremely difficult to fit this profile properly. In this case, the width and height of the profile is caused by a very small range of laboratory speeds and therefore spurious cancellations of nearby and partially overlapping velocity basis functions cannot account for its features to the degree shown in Fig. 1.

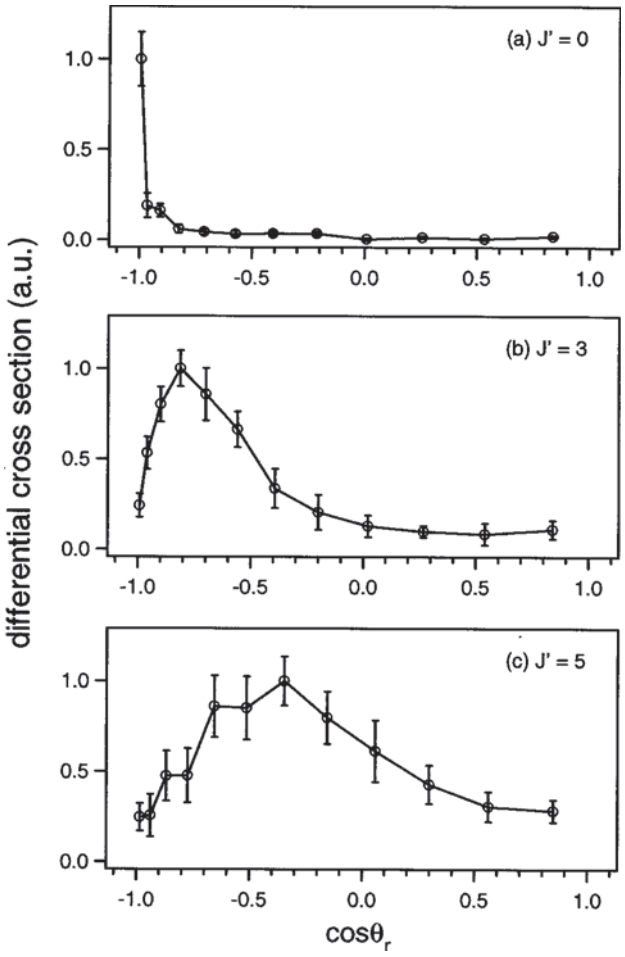

FIG. 2. Angular distributions derived from the time-of-flight profiles shown in Fig. 1. The solid lines are guides to the eye.

From consideration of the velocity resolution of the instrument we conclude we are justified to use twelve basis functions spanning the whole laboratory speed range corresponding to reactive product. Examination of the covariance matrix from the linear least-squares fit to the signal suggests that a slightly larger number of basis functions, between 13 and 15, could be used to fit the time-of-flight profiles before there is significant covariance between adjacent velocity basis functions. We have chosen to adopt the more conservative approach and only use the number of velocity basis functions that our knowledge of the instrument function prescribes. This number of basis functions leads to an angular resolution of about 6° for backward scattering and about 13° for forward scattering.

Figure 2 shows the angular distributions derived from the core-extracted time-of-flight profiles of Fig. 1. Twelve points span the whole center-of-mass angular range. The error bars for each point represent the 1σ uncertainty associated with both random (Poisson) noise in the signal and reproducibility errors obtained from at least five measurements of each rovibrational state. We should stress the fact that these error bars are therefore a direct measure of our ability to measure these angular distributions repeatedly with our instrument as opposed to just providing the error or variance associated with a single fit to the signal.

As Fig. 2 shows, there is a clear and systematic change in the peak position and breadth of the angular distributions as the rotational energy of the product increases. For HD ($v'=2$, $J'=0$) the differential cross section is strongly peaked in the backward direction. For HD ($v'=2$, $J'=3$) the peak of the distribution has shifted to ~144° and a wider range of angles around this value contribute to product scattering. Finally, for HD ($v'=2$, $J'=5$), the most probable scattering angle has moved to ~115°, and a sizable amount of scattering occurs over much of the angular range. The same trend was found in our previous study of the HD ($v'=1$, J') angular distribution at similar collision energies.[7]

IV. DISCUSSION AND CONCLUSIONS

For the $H+D_2$ reaction at a collision energy of 1.55 eV we have conducted differential cross section measurements for HD ($v'=2$, $J'=0,3,5$) products using the photoloc technique. Core extraction allows direct inversion of time-of-flight data into product center-of-mass angular distributions with an angular resolution of about 6° for backward scattering changing to 13° for forward scattering. These measurements have been possible after further refinement of the experimental protocol, which required a careful choice of the experimental conditions as well as multiple experimental checks to ensure time-of-flight profiles are devoid of experimental artifacts. Comparison of the present set of angular distributions with HD ($v'=1$, J') measurements previously obtained in our laboratory shows the same overall trends with product rotational quantum number. Specifically, we find strong backscattering for low J' and a gradual shift of the angular distribution toward smaller angles with increased product rotational quantum number.

The lack of theoretical calculations for this reaction system at our collision energies precludes us from a direct comparison with either quantum mechanical calculations or with the more economical quasiclassical trajectory method. As we already mentioned in our previous study of the angular distributions for HD ($v'=1$, J') states, we hope these measurements will be put to the test against the most accurate calculations for the $H+D_2$ including effects such as the geometric phase. As predicted by Kuppermann and coworkers,[25–27,55–60] our collision energies should be sufficiently high to observe the effects of this phenomenon, especially if comparison between experiment and theory is possible at the level of rovibrational-state-resolved differential cross sections. The question remains open, however, as to whether our differential cross section measurements are sensitive to these effects.

A. Comparison of differential cross sections

It is of interest to compare our differential cross sections to those reported at different collision energies. The state-resolved angular distributions of Schnieder *et al.* at 1.28 eV[21] for the same internal states show a similar dependence of the angular distribution with product rotational quantum number. For this lower collision energy, the angular distributions peak at ~170–180° for $J'=0$, ~140° for $J'=3$, and ~120° for $J'=5$. However, the differential cross section for $J'=0$, from the work of Schnieder *et al.* at 1.28 eV shows a broader range of angles, extending down to ~120°, than what we have observed. Similarly, recent measurements by the same group at 2.2 eV (Ref. 45) show angular distributions peaking at ~180° for HD ($v'=2$, $J'=0$), ~150° for for HD ($v'=2$, $J'=3$), and ~115° for for HD ($v'=2$, $J'=6$). The experimental differential cross section for HD ($v'=2$, $J'=3$), however, shows a clear additional local maximum at 180°, similar to the one we found for HD ($v'=1$, $J'=5$) at 1.70 eV. As much as angular distributions at different collision energies can be compared, the same qualitative trends are found in the experimental studies carried out by us and by Schnieder and co-workers.

TABLE II. Summary of HD (v',J') product states probed until the present.

Collision energy (eV)[a]	Vibrational quantum number v'	Rotational quantum number J'	HD (v',J') internal energy (eV)	Most probable scattering angle (deg.)
1.71[b]	1	1	0.694	170°
1.70[b]	1	5	0.839	133°
1.66[b]	1	8	1.047	100°
1.56[c]	2	0	1.109	175°
1.55[c]	2	3	1.169	144°
1.53[c]	2	5	1.257	115°

[a]Collision energy spread estimated to be ±50 meV for all states shown here (see Ref. 8).
[b]From Ref. 7.
[c]This work.

For the purpose of comparison with our previously reported HD ($v'=1$, J') differential cross section data we have included in Table II a summary of some of the information inferred from our measurements. Even though the collision energy for both sets of measurements is slightly different there are certain trends likely to be independent of this difference. Such is the case, for example, for the lack of correlation between the coarse features of the angular distributions (i.e., most probable scattering angle) and the total internal energy (vibrational plus rotational) of the diatomic product. This lack of correlation is best exemplified by rows three and four in Table II, which pertain to two almost isoenergetic states. Despite this similarity in regard to total internal energy, the angular distributions are at the two extremes of what we have observed thus far for this reaction: HD($v'=1$, $J'=8$) peaks at ~100° whereas HD ($v'=2$, $J'=0$) peaks at ~175°. Further examination of Table II reveals that for either vibrational manifold, the dependence of the most probable scattering angle with product rotational quantum number is very similar. It thus seems that the primary and most important variable correlated with the peak of the angular distribution is the product rotational quantum number. Product vibrational excitation seems to be much less important, that is, different vibrational manifolds show the same overall trends in the angular distributions.

From these observations, we conclude that for HD ($v'=2$, J') product a rough correlation also exists between the peak and shape of the differential cross section and the final total angular momentum of the diatomic product. Following the analysis based on the line-of-centers with nearly elastic specular scattering (LOCNESS) model proposed previously,[7] we have plotted the most probable scattering angle versus the

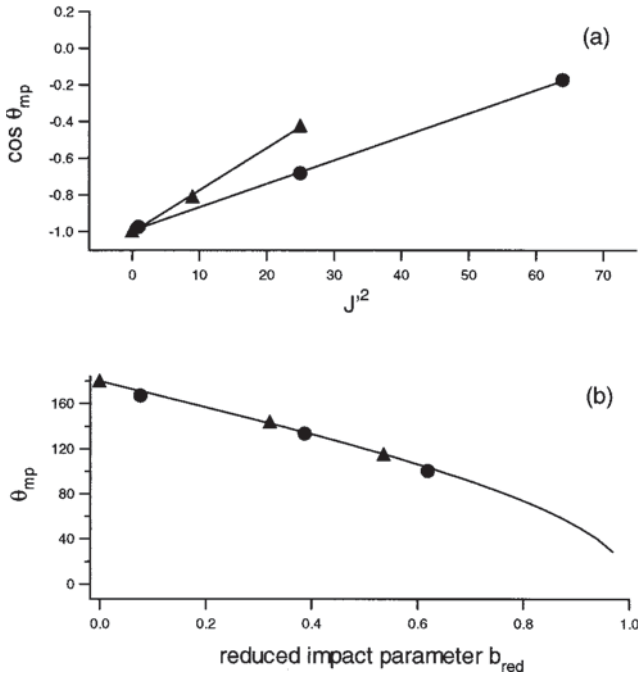

FIG. 3. (a) Correlation between the most probable scattering angle θ_{mp} and product rotational angular momentum J'. Circles correspond to HD ($v'=1$) and triangles to HD ($v'=2$). Note the different slopes indicative of a different hard-sphere radius for each vibrational manifold. (b) Relationship between most probable scattering angle θ_{mp} and reduced impact parameter b_{red} deduced from the correlation shown in (a). The solid line represents the hard-sphere limit, given by $\cos\theta_{mp}=2b_{\mathrm{red}}^2-1$.

square of the rotational quantum number for the HD ($v'=2$, J') angular distributions. This plot is presented in Fig. 3. The correlation between the most probable angle and J'^2, and thus between b and J' if a hard-sphere deflection function is assumed, is also present in the $v'=2$ case. This time, however, the most probable scattering angle decreases faster with J' than in the $v'=1$ case. Because $b_{\mathrm{red}}=b/d$, we are led to interpret this result as arising from a smaller hard sphere radius d for $v'=2$ compared to $v'=1$. This result is expected in view of the fact that vibrational excitation of the product is more probable for small impact parameters for which the conversion of initial translational energy into vibrational energy of the product is more facile. In other words, the opacity function leading to vibrationally excited product has an earlier cutoff for products with increased vibrational energy. Inspection of the state-resolved differential cross section measurements of Schnieder *et al.* at 1.28 eV (Ref. 21) and 2.20 eV (Ref. 45) shows the same trend of the angular distributions for the same rotational quantum number in different vibrational levels. It thus seems that similar collision dynamics are governing the outcome of this reaction despite the collision energy differences between these two independent experimental studies.

B. Predictions of the LOCNESS model

The assumptions built into the LOCNESS model for this reaction lack a strict justification. Therefore, its predictions should be taken as mere guides for a more detailed elucidation of the dynamics of this reaction. The assumption, for example, of a hard sphere deflection function is the simplest approximation that can be made but we should remember that it is also the expected limit for a direct reaction with similar entrance and exit valleys (i.e., similar reagent and product channel impact parameters) as is the case for the hydrogen exchange reaction. Moreover, this assumption about the nature of the deflection function predicts that the angular distribution should be directly related to the opacity function for reaction. Theoretical calculation of the opacity functions for different product channels and direct comparison with the angular distributions should therefore provide a way of quantitatively assessing the validity of these approximations. Indeed, the recent quantum-mechanical calculations accompanying the experimental work of Schnieder *et al.* at 2.2 eV (Ref. 45) show the opacity function for reaction as a function of J'. For HD products with $v'<3$ the relationship between J_{total} (or impact parameter b) and J' is quite clear. Additionally, the opacity functions broaden with increased product rotation, which is ultimately translated into a broadening of the product angular distribution. Nevertheless we are encouraged that the very simple arguments of the LOCNESS model can be used to rationalize the experimental results in a way consistent with what is known about this reaction system.

The LOCNESS model can also be used to make straightforward predictions on some of the features of other experimental observables, such as the smallest scattering angle and the corresponding cutoff in the product rotational distribution for a given product vibrational state. The presence of a barrier of at least 0.41 eV along the minimum energy path to reaction already limits the maximum reduced impact parameter energetically accessible to a value given by

$$b_{\mathrm{red}}^{\max}=\left(1-\frac{E_0}{E_T}\right)^{1/2}, \tag{1}$$

where E_0 is the minimum energy barrier and E_T is the total energy available. Beyond this value, no sufficient energy exists to cross the reaction barrier. For the two sets of angular distributions measured so far by us, this value as given by Eq. (1) is roughly 0.85. At this maximum impact parameter we expect that only trajectories going through a linear transition state are able to cross into the product valley because most of the energy is locked into centrifugal energy, whose motion is perpendicular to the line of centers. Also, by assuming a hard-sphere deflection function, the differential cross section should not show pronounced peaks beyond 60–65°. This lower limit to the scattering angle has been strictly observed in all state-to-state differential cross sections measured for this reaction system.

At the same time, for collisions at zero impact parameter we expect to have the broadest range of transition state geometries leading to reaction. In Fig. 4 we have plotted the value of the reduced impact parameter for reaction versus the maximum angle of approach expected from the angle-dependent barrier for this reaction at a given collision energy. The angle-dependent barrier to reaction can be obtained from the LSTH PES and has been given by several authors.[16,61,62] For the purpose of the calculations presented here we have fitted the LSTH angle-dependent reaction barrier to a second-order polynomial in cos γ of the form

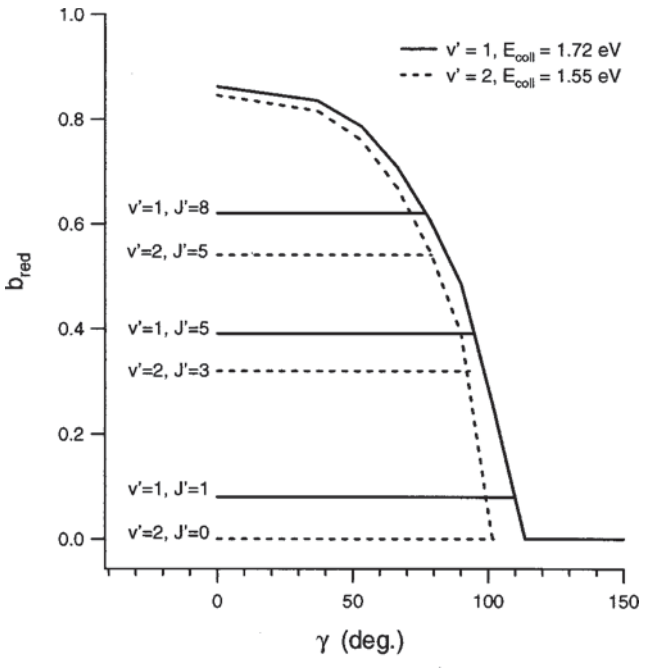

FIG. 4. Reduced impact parameter b_{red} vs maximum angle of approach γ taking into account the energy-dependent barrier present in this reaction. Each horizontal line represents a given HD rovibrational state. From the figure it is clear that each vibrational manifold converges to a different maximum rotational quantum number for $b_{\mathrm{red}}^{\mathrm{max}}$, namely, $J'=11$ for $v'=1$ and $J'=8$ for $v'=2$.

$$V_b = V_b^0 + V_b^1 \cos\gamma + V_b^2 \cos^2\gamma, \tag{2}$$

where γ is the angle of attack of the H atom, that is, the H–D–D angle, measured from 0° for collinear approach. The parameters $V_b^0 = 1.32\,\mathrm{eV}$, $V_b^1 = -1.30\,\mathrm{eV}$, and $V_b^2 = 0.40\,\mathrm{eV}$, are obtained from the polynomial fit to the *ab initio* points.

For zero impact parameter collisions, approach angles of up to 110° for HD ($v'=1$) and 100° for HD ($v'=2$) are energetically possible. At our collision energies, it is thus expected that small impact parameter trajectories inserting into the D–D bond can start competing with a more direct mechanism in which the approach of the H atom is restricted to a narrower range of angles of attack. Consequently, we are led to believe that severe deviations from the expectations of the LOCNESS model might be observed for products for low rotational quantum numbers, specially $J'=0$. An evident signature of these deviations would be the appearance of a forward-scattered peak in the differential cross section. We do not observe this behavior, however.

In Fig. 4 we also show the reduced impact parameter for HD ($v'=1,2$, J') states deduced from the correlation between most probable scattering angle and rotational quantum number (see Fig. 3). The two ladders of rotational quantum numbers, i.e., the solid line for $v'=1$, and the dashed line for $v'=2$, must terminate at the maximum allowed reduced impact parameter. This condition provides us with a cutoff for each rotational distribution. For $v'=1$, the maximum rotational quantum number predicted is $J'=11$ and for $v'=2$ it is $J'=8$. Both values are significantly lower than the maximum rotational quantum number allowed by energy conservation. This behavior also suggests that an instructive way of looking at the rotational distributions for a given collision energy is to plot them with respect to a reduced variable, namely J/J_{max}, where J_{max} is the maximum rotational quantum number allowed within the framework of the LOCNESS model. As explained above, J_{max} has been obtained from the measurement of the angular distributions as a function of rotational quantum number, an observable that does not depend on the integral cross section measurement. By examining the experimental data in this manner, we might discern any differences in reaction mechanisms leading to the reaction products in different vibrational levels.

It seems that the LOCNESS model can qualitatively explain the differences in the shift of the angular distributions from backward toward side scattering with increasing J' for both vibrational levels. In this model nearly specular scattering occurs along the line of centers. We find that the shift is more pronounced for $v'=2$, which implies a smaller range of impact parameters leading to reaction for $v'=2$ compared to $v'=1$. The same qualitative trends are also found in experimental data taken by Schnieder *et al.* at 1.28 and 2.20 eV. We have also examined in some detail some of the immediate predictions of the LOCNESS model regarding the smallest scattering angle and the cutoff in the rotational distributions. We suggest that this behavior might be general for exchange reactions that proceed by direct abstraction.

ACKNOWLEDGMENTS

The authors thank James D. Ayers, Zee Hwan Kim, and Michael A. Everest for valuable discussions. We are also grateful to Professor Luis Bañares for sending us a copy of Ref. 45 prior to publication. The National Science Foundation is gratefully acknowledged for financial support under Grant No. CHE-93-22690 and CHE-99-00305.

[1] D. G. Truhlar and R. E. Wyatt, Annu. Rev. Phys. Chem. **27**, 1 (1976).
[2] J. Geddes, Contemp. Phys. **23**, 233 (1982).
[3] R. D. Levine, Int. J. Chem. Kinet. **18**, 9 (1986).
[4] G. C. Schatz, Annu. Rev. Phys. Chem. **39**, 317 (1988).
[5] W. H. Miller, Annu. Rev. Phys. Chem. **41**, 245 (1990).
[6] H. Buchenau, J. P. Toennies, J. Arnold, and J. Wolfrum, Ber. Bunsenges. Phys. Chem. **94**, 1231 (1990).
[7] F. Fernández-Alonso, B. D. Bean, and R. N. Zare, J. Chem. Phys. **111**, 1035 (1999).
[8] F. Fernández-Alonso, B. D. Bean, and R. N. Zare, J. Chem. Phys. **111**, 1022 (1999).
[9] W. R. Simpson, A. J. Orr-Ewing, T. P. Rakitzis, S. A. Kandel, and R. N. Zare, J. Chem. Phys. **103**, 7299 (1995).
[10] N. E. Shafer, H. Xu, R. P. Tuckett, M. Springer, and R. N. Zare, J. Phys. Chem. **98**, 3369 (1994).
[11] N. E. Shafer, A. J. Orr-Ewing, W. R. Simpson, H. Xu, and R. N. Zare, Chem. Phys. Lett. **212**, 155 (1993).
[12] J. Geddes, H. F. Krause, and W. L. Fite, J. Chem. Phys. **56**, 3298 (1972).
[13] G. H. Kwei and V. W. S. Lo, J. Chem. Phys. **72**, 6265 (1980).
[14] R. Götting, H. R. Mayne, and J. P. Toennies, J. Chem. Phys. **80**, 2230 (1984).
[15] R. Götting, H. R. Mayne, and J. P. Toennies, J. Chem. Phys. **85**, 6396 (1986).
[16] P. Siegbahn and B. Liu, J. Chem. Phys. **68**, 2457 (1978).
[17] D. G. Truhlar and C. J. Horowitz, J. Chem. Phys. **68**, 2466 (1978).
[18] S. A. Buntin, C. F. Giese, and W. R. Gentry, J. Chem. Phys. **87**, 1443 (1987).
[19] R. E. Continetti, B. A. Balko, and Y. T. Lee, J. Chem. Phys. **93**, 5719 (1990).
[20] L. Schnieder, K. Seekamp-Rahn, J. Borkowski, E. Wrede, K. H. Welge, F.

J. Aoiz, L. Bañares, M. J. D'Mello, V. J. Herrero, V. Séez Rábanos, and R. E. Wyatt, Science **269**, 207 (1995).
[21] L. Schnieder, K. Seekamp-Rahn, E. Wrede, and K. H. Welge, J. Chem. Phys. **107**, 6175 (1997).
[22] E. Wrede and L. Schnieder, J. Chem. Phys. **107**, 786 (1997).
[23] L. Bañares, F. J. Aoiz, V. J. Herrero, M. J. D'Mello, B. Niederjohann, K. Seekamp-Rahn, E. Wrede, and L. Schnieder, J. Chem. Phys. **108**, 6160 (1998).
[24] F. J. Aoiz, L. Bañares, M. J. D'Mello, V. J. Herrero, V. Sáez Rábanos, L. Schnieder, and R. E. Wyatt, J. Chem. Phys. **101**, 5781 (1994).
[25] A. Kuppermann and Y.-S. M. Wu, Chem. Phys. Lett. **205**, 577 (1993).
[26] Y.-S. M. Wu and A. Kuppermann, Chem. Phys. Lett. **235**, 105 (1995).
[27] A. Kuppermann, in *Dynamics of Molecules and Chemical Reactions*, edited by R. E. Wyatt and J. Z. H. Zhang (Marcel Dekker, New York, 1996).
[28] M. P. de Miranda, D. C. Clary, J. F. Castillo, and D. E. Manolopoulos, J. Chem. Phys. **108**, 3142 (1998).
[29] N. E. Shafer-Ray, A. J. Orr-Ewing, and R. N. Zare, J. Phys. Chem. **99**, 7591 (1995).
[30] W. R. Simpson, A. J. Orr-Ewing, and R. N. Zare, Chem. Phys. Lett. **212**, 163 (1993).
[31] W. R. Simpson, T. P. Rakitzis, S. A. Kandel, T. Lev-On, and R. N. Zare, J. Phys. Chem. **100**, 7938 (1996).
[32] S. A. Kandel, T. P. Rakitzis, T. Lev-On, and R. N. Zare, J. Chem. Phys. **105**, 7550 (1996).
[33] S. A. Kandel, T. P. Rakitzis, T. Lev-On, and R. N. Zare, Chem. Phys. Lett. **265**, 121 (1996).
[34] S. A. Kandel, T. P. Rakitzis, T. Lev-On, and R. N. Zare, J. Phys. Chem. A **102**, 2270 (1998).
[35] H. L. Kim, M. A. Wickramaaratchi, X. Zheng, and G. E. Hall, J. Chem. Phys. **101**, 2033 (1994).
[36] A. J. Alexander, F. J. Aoiz, L. Bañares, M. Brouard, J. Short, and J. P. Simons, J. Phys. Chem. A **101**, 7544 (1997).
[37] M. Brouard, D. W. Hughes, K. S. Kalogerakis, and J. P. Simons, J. Phys. Chem. A **102**, 9559 (1998).
[38] T. P. Rakitzis, S. A. Kandel, and R. N. Zare, J. Chem. Phys. **107**, 9382 (1997).
[39] T. P. Rakitzis, S. A. Kandel, T. Lev-On, and R. N. Zare, J. Chem. Phys. **107**, 9392 (1997).
[40] A. J. Orr-Ewing, W. R. Simpson, T. P. Rakitzis, S. A. Kandel, and R. N. Zare, J. Chem. Phys. **106**, 5961 (1997).
[41] S. A. Kandel, Ph.D. thesis, Stanford University, 1998.
[42] H. Xu, N. E. Shafer-Ray, F. Merkt, D. J. Hughes, M. Springer, R. P. Tuckett, and R. N. Zare, J. Chem. Phys. **103**, 5157 (1995).
[43] E. Wrede, L. Schnieder, K. H. Welge, L. Bañares, and V. J. Herrero, Chem. Phys. Lett. **265**, 129 (1997).
[44] E. Wrede, L. Schnieder, K. H. Welge, F. J. Aoiz, L. Bañares, V. J. Herrero, B. Martínez-Haya, and V. Sáez Rábanos, J. Chem. Phys. **106**, 7862 (1997).
[45] E. Wrede, L. Schnieder, K. H. Welge, F. J. Aoiz, L. Bañares, J. F. Castillo, B. Martínez-Haya, and V. J. Herrero, J. Chem. Phys. **110**, 9971 (1999).
[46] A. I. Boothroyd, W. J. Keogh, P. G. Martin, and M. R. Peterson, J. Chem. Phys. **104**, 7139 (1996).
[47] N. C. Blais and D. G. Truhlar, Chem. Phys. Lett. **162**, 503 (1989).
[48] P. M. Regan, S. R. Langford, A. J. Orr-Ewing, and M. N. R. Ashfold, J. Chem. Phys. **110**, 281 (1999).
[49] K.-D. Rinnen, D. A. V. Kliner, R. N. Zare, and W. M. Huo, Isr. J. Chem. **29**, 369 (1989).
[50] K.-D. Rinnen, M. A. Buntine, D. A. V. Kliner, R. N. Zare, and W. M. Huo, J. Chem. Phys. **95**, 214 (1991).
[51] K. P. Huber and G. Herzberg, *Molecular Spectra and Molecular Structure. IV. Constants of Diatomic Molecules* (Van Nostrand Reinhold, New York, 1979).
[52] N. C. Blais and D. G. Truhlar, Chem. Phys. Lett. **102**, 120 (1983).
[53] W. H. Press, B. P. Flannery, S. A. Teukolsky, and W. T. Vetterlich, *Numerical Recipes in Fortran* (Cambridge University Press, Cambridge, 1986).
[54] F. Fernández-Alonso, B. D. Bean, and R. N. Zare (unpublished).
[55] B. Lepetit and A. Kuppermann, Chem. Phys. Lett. **166**, 581 (1990).
[56] Y.-S. M. Wu, A. Kuppermann, and B. Lepetit, Chem. Phys. Lett. **186**, 319 (1991).
[57] Y.-S. M. Wu and A. Kuppermann, Chem. Phys. Lett. **201**, 178 (1993).
[58] A. Kuppermann, Faraday Discuss. Chem. Soc. **110**, 212 (1998).
[59] A. Kuppermann, Faraday Discuss. Chem. Soc. **110**, 215 (1998).
[60] A. Kuppermann, Faraday Discuss. Chem. Soc. **110**, 213 (1998).
[61] R. D. Levine and R. B. Bernstein, Chem. Phys. Lett. **105**, 467 (1984).
[62] M. H. M. Janssen and S. Stolte, J. Phys. Chem. **91**, 5480 (1987).